Improving Wireless Simulation Through Noise Modeling

HyungJune Lee[†], Alberto Cerpa[‡], and Philip Levis[†]

[†]Computer Systems Laboratory
Stanford University
Stanford, CA 94305

abbado@stanford.edu
pal@cs.stanford.edu

[‡]School of Engineering
University of California, Merced
Merced, CA 95344

acerpa@ucmerced.edu

Abstract

We investigate how to efficiently and accurately simulate wireless packet delivery. Starting from recent experimental results that have quantified signal-to-noise ratio (SNR) curves, temporal variations in propagation strength, and the effects of hardware variations, we model packet delivery using SNR. We experimentally measure noise in many different environments and propose three algorithms to simulate noise from these traces. We evaluate these algorithms in comparison to existing simulation approaches used in EmStar, TOSSIM, and ns-2 using the Kantorovich-Wasserstein distance on conditional packet delivery functions. We demonstrate that using a closest-fit pattern matching (CPM) noise model can capture complex temporal dynamics which existing approaches do not, increasing packet simulation fidelity by a factor of 2 for good links and a factor of 3 for intermediate links. Furthermore, as our models are generated from real-world traces, they are not bound to specific environments and can be easily applied to new ones.

1. INTRODUCTION

Simulation is a critical part of developing, testing, and evaluating sensornet protocols and systems. Having complete control of the simulated environment allows us to run reproducible experiments, explore parameter spaces, and disambiguate causes of error or undesirable behavior. The inherent difficulty in developing robust sensornet codes has led many tools to focus on system dynamics through real-code simulation [2, 11, 14, 21].

Very accurate system simulation allows users to test code paths. It does not, however, promise a representative execution environment. First and foremost, low-power wireless networks have many complex, rare, and difficult behaviors and that protocols must address properly in order to be effective in practice [5, 6, 9, 20, 23]. Early studies noted that packet delivery rates are highly variable over distance [9, 23]. Many existing simulators have used the high-level packet delivery data from these experiments in their network models [11, 14]. While this approach allows simulators such as TOSSIM and EmStar to have packet delivery behavior similar to the real world. However, as these simulators simulate the loss itself rather than its causes, they are unable to easily or accurately model novel environments, concurrent transmissions, or variable packet sizes.

Recent investigations into low-cost radio hardware has distinguished how many different factors, such as hardware calibration, interference, and orientation affect packet delivery [19]. In particular, these and other results [16, 20] have verified that packet delivery follows a simple SNR curve. Furthermore, these studies have shown that the RSSI of received packets (the S of the SNR) is often very stable over long periods. Taken together, these observations point at the causes of temporal variations in packet loss and bursty connectivity. Hardware variations cause node pairs to have different SNR curves, but for any given pair the curve is precise. As RSSI is generally stable over short periods, it is reasonable to conclude that the missing piece of the RF simulation puzzle is the environmental noise.

Unfortunately, simulating environmental noise is hard. Unlike hardware-based noise, which is typically modeled as additive white Gaussian noise (AWGN), environmental noise is often from packet-based devices. Section 2 shows how packet based noise appears as brief, strong, short-lived noise spikes which can be temporally correlated. To simulate this noise, we gather 1kHz noise traces using current 802.15.4 sensor node platforms and use these traces to generate statistical models of noise using three techniques, presented in Section 3: probabilistic sampling, closest-fit pattern matching (CPM), and a non-Gaussian random process. We simulate radio packet delivery with these noise models using an SNR/PRR curve. Whenever a simulated node receives a packet, it samples a noise reading from one of these models to determine the SNR and computes the packet delivery probability.

We have implemented these approaches in the TOSSIM simulator of TinyOS 2.0. Section 4 evaluates how well the algorithms as well as wireless protocol simulators such as EmStar [11], TOSSIM 1.x [14], TOSSIM 2.x [4], and NS-2 [1] simulate packet delivery dynamics for good, intermediate, and poor links. To capture temporal packet dynamics, we evaluate simulation accuracy using conditional packet delivery functions (CPDFs), which describe the probability a packet will be delivered successfully after n consecutive failures or successes. We compare CPDFs using the Kantorovich-Wasserstein distance [12]. Our results indicate

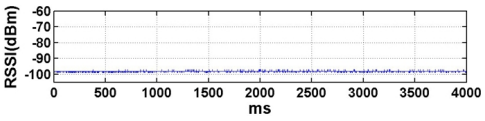

(a) Lake Lagunita, channel 26

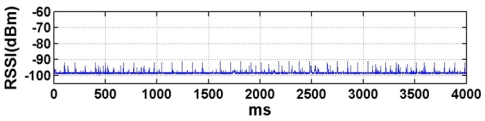

(b) Lake Lagunita, channel 18

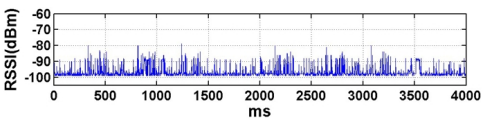

(c) Meyer Library, channel 18

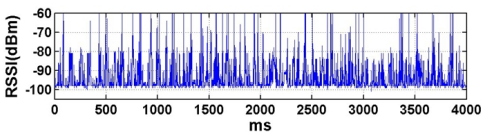

(d) Meyer Library, channel 18, during nearby heavy 802.11 use

Figure 1: 4 second 1kHz noise traces of 802.15.4 channel 26 and 18 measured at an outdoor park and in a library with dense 802.11b coverage. Noise sources in the 2.4GHz band are discrete but show significant temporal correlation.

that existing techniques are sufficient for environments with little noise, but for noisy environments closest-fit pattern matching significantly outperforms all other approaches.

We have gathered noise traces for a variety of environments, including busy and quiet indoor office environments, outdoor areas with 802.11 connectivity, and outdoor environments with no interfering traffic (the Grand Canyon). Section 6 discusses the implications and limitations our approaches as well our planned directions of future work. Our results suggest that an effective route towards accurate wireless simulation is to simply *measure* a diverse set of environments and generate statistical models of them.

2. BACKGROUND

Accurately simulating wireless packet delivery is a long-standing challenge in sensornet research. Early studies [17] used a unit-disc model, which defines transmission range as a simple disc of binary connectivity; nodes within a range r successfully receive packets, while those outside r do not. This model, while simple to implement and reason about, has little basis in reality. Experimental studies have shown that connectivity varies tremendously over distance [10, 23] and that many links fall into a "grey region" of intermediate packet delivery success.

In response to the observation that connectivity is more complex than what simple disc or RF propagation models (such as those used in ns2 [1]) can express, sensornet simulators have for the most part adopted an empirical approach. Rather than try to model the underlying causes of RF connectivity, such as interference, noise, and RF propagation, an empirical approach merely recreates packet-level behavior. For example, TOSSIM takes inter-node distances and samples from a packet reception rate (PRR) distribution to determine the connectivity between a pair of nodes [14]. This simple approach can capture a large number of real-world complexities, such as link asymmetries and highly variable spatial connectivity. However, it also makes simplifying assumptions that do not hold in practice. First and foremost, this approach assumes that every link is independent (they are sampled independently from the distance distribution), while real networks tend to have "bad" nodes with poor connectivity. This simplification causes discrepancies between simulation and testbed experiments, such as those observed in the Trickle algorithm [15].

The EmStar system [11] avoids the independence problems of TOSSIM by having one of its radio models using PRR values measured in real-world networks [5]. This has the benefit of capturing effects such as poor receivers. The cost is that it can only simulate networks for which PRR has been measured. The EmStar and TOSSIM approaches assume that packet losses are independent (PRR does not change), but experimental results have shown that PRR varies significantly over time [5, 6].

Recent studies have begun to shed light on the underlying causes of the complex packet delivery behavior observed in real networks [19]. One important observation from these studies is that for a given node pair, there is a crisp SNR/PRR curve. Effects such as a wide reception grey region are caused by different pairs having different curves and variations in observed signal strength. These effects can be captured with reasonable accuracy through a hardware covariance matrix [24].

Experimental studies of current sensornet platforms, such as the micaZ and telosB, have shown that signal strength is stable over short periods of time, but can have longer-term variations due to environmental conditions [16, 20]. However, computing PRR from an SNR curve requires the noise as well as the signal. As sensornets often operate in unlicensed ISM bands, their spectrum is crowded with many conflicting transmitters. 2.4 GHz, the band used by micaz, telos, and imote2 nodes, is particularly crowded, as it is also occupied by 2.4 GHz phones, 802.11b/g, microwave ovens, and Bluetooth, all of which interfere significantly. Without these considerations, SNR-based simulation models are fundamentally limited in accuracy.

The hypothesis of this paper is that coming up with an efficient and effective model of environmental noise will allow a sensornet simulator to accurately model packet delivery using an SNR/PRR curve. We leverage the observations and advances of prior work to achieve this goal. From Zuniga *et al.*'s experimental work [24] we borrow the idea of hardware covariance matrices to govern the SNR curve of a node pair. From EmStar we borrow the idea of measuring real environments to derive a representative model. Once we have derived a per-node noise model, we plug it and the RSSI of a transmitter into a SNR curve to compute packet delivery probability. Simulating noise allows us to capture short-term connectivity variations, such as those caused by a large burst of 802.11 traffic.

The challenge in simulating 2.4GHz noise is that it does not follow a clean and elegant mathematical model. Because much of the interference is 802.11 traffic, it has a highly bimodal behavior: an 802.11 node is either transmitting or

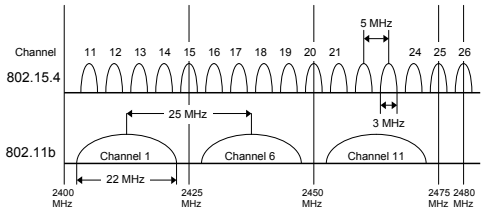

Figure 2: 802.11b and 802.15.4 spectrum utilization. Channel 18 in 802.15.4 heavily overlaps with 802.11b channels, while channel 26 in 802.15.4 has no overlap with 802.11b spectrum.

not. Instead of a Gaussian process or wave, transmissions are a discrete signal with highly variable temporal characteristics. Figure 1 shows four noise traces from different environments on 802.15.4 channel 18. Lake Lagunita at Stanford is almost free of 802.11b interferences and other noise sources. On the other hand, Stanford Meyer library has many 802.11b access points and so has severe 802.11b interference. The periodic peak values in the plots are 802.11b beacon packets at a frequency 9.765 Hz (0.1024 sec). The next section describes three approaches to statistically modeling 2.4GHz noise, and Section 4 evaluates how well these approaches reflect real-world behavior in comparison to commonly used simulators.

3. NOISE CHARACTERIZATION

This section describes three approaches to statistically characterize noise traces. The first approach, *naive sampling*, generates a probability distribution of a noise trace and simply samples from this distribution. Naive sampling is fast and simple, but makes the assumption that noise samples are independent. The second approach, *closest-fit pattern matching* (CPM), computes the conditional probability distribution of noise values given n previous noise readings. It generates a noise value based on the matching series and defaults to the mode when no measured series matches. The third approach uses a non-Gaussian random model with the *correlation distortion method* in order to describe noise as a random process. This has the advantage that it can capture temporal dynamics, but is computationally expensive and has difficulty with signals that are highly non-Gaussian.

3.1 Measuring Noise

To measure environmental noise, we wrote a TinyOS application that samples RF energy at 1kHz by reading the RSSI register of the CC2420 radio. The register contains the average RSSI over the past 8 symbol periods (125μs). The application logs this data to flash for a fixed period of time ($3 * 2^{16}$ samples, so $\approx$ 197s). A PC application reads the data off of the mote. We sampled noise on different radio channels in a wide range of environments, including inside WiFi enabled buildings (Meyer Library at Stanford), in outdoor WiFi enabled areas (Lake Lagunita at Stanford), in outdoor quiet areas (Grand Canyon), and during controlled tests (a large HTTP download in Meyer Library).

Figure 1 shows 4 second periods from four gathered noise traces. These traces show three key characteristics of noise in the 2.4GHz band. First, noise tends to have discrete spikes, which are as much as 40dBm above the noise floor. These spikes typically but not always represent transmissions from copresent wireless packet networks. As Figure 2 shows, 802.11 shares spectrum with the 802.15.4 radios used in several sensor platforms. Second, many of these spikes are periodic. For example, 802.11b base stations transmit beacons every 0.1024s. Third, noise is temporally correlated: there are periods of activity and periods of quiet.

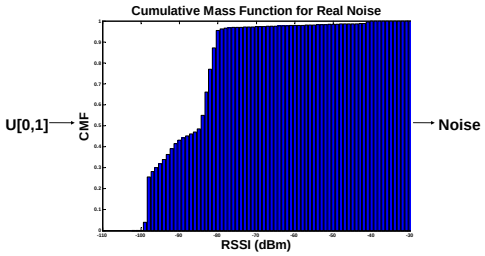

(a) Simulating noise with naive sampling.

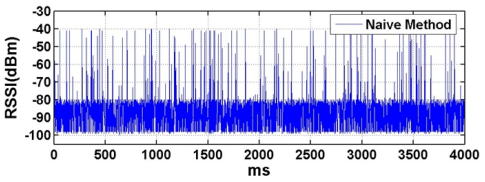

(b) Sample noise trace from naive sampling using heavy traffic Meyer trace.

Figure 3: Simulating noise with naive sampling. By generating a uniformly distributed random variable in [0,1], a noise sample can be derived by filtering with CMF function of measured noise.

The rest of this section describes three approaches to modeling 2.4GHz noise: naive sampling, closest-fit pattern matching, and the correlation distortion method.

3.2 Naive Sampling

Because copresent packet networks represent discrete event sources, probabilistic sampling is a simple way to model noise. This approach works by computing the distribution of noise values and sampling from the distribution whenever a noise value is needed. This approach has the benefit that generating the model and taking samples from it is very fast.

Assuming that each noise sample is independent, simulating a noise trace can be reduced to generating random variables. Once a cumulative mass function (CMF) of target data is prescribed, the same distribution of simulated data can be achieved by filtering uniformly distributed random numbers as inputs by the inverse CMF in Figure 3. The target distribution does not need to be continuous for the above method to work; it can be discrete. The probability mass function (PMF) of the simulated data is nearly identical to the target data.

While simple and fast, this method neglects crucial information such as time-dependence. Noise has temporal correlation, and making samples independent breaks this correlation. In theory, this means that if real noise has bursts of interference that causes bursts of packet losses, a naïve sampling model may not be able to capture this behavior. On the other hand, it may be that this limitation ends up having minimal effects on the final simulation behavior. We therefore consider this approach to be a baseline measure-

Bin	1	2	3	...	16
RSSI(dBm)	-102∼ −98	-97∼ −93	-92∼ −88	...	-27∼ −23

Table 1: Closest-fit pattern matching further discretizes noise values in order to shrink its state space.

ment for noise simulation.

3.3 Closest-fit Pattern Matching (CPM)

Unlike naïve sampling, which generates independent noise values, closest-fit pattern matching (CPM) uses a probability distribution of noise values given k previous noise values. One problem CPM faces is an exploding state space: if noise can take ≈60 values (-100 to -40 dBm), then CPM with a window of $k = 10$ has a state space of 60^{10}, or $\approx 6 \cdot 10^{17}$. As our traces have only $\approx 2 \cdot 10^5$ samples, very few patterns will be populated. We therefore further discretize the RSSI values, as shown in Table 1.

Each data point in the CPM model is a PDF of the observed noise values given k previous values. To determine the noise value of time n_t, CPM samples from the PDF associated with $n_{t-1}, n_{t-2}, \ldots n_{t-k}$. If there is no PDF associated with this noise series, CPM samples from the most common PDF (the mode). CPM bootstraps from the measured trace: first k noise values are simply the first k samples from the real-world measurements.

In the degenerate case of $k = 0$, CPM is equivalent to naïve sampling. There is a tradeoff in how large a k is used. A large k allows CPM to capture longer term periodicities. However, as the state space grows at $O(r^k)$ where r is the number of discretized RSSI readings, but the number of samples does not increase, the probability that any sequence exists goes down exponentially. This is a basic overfitting problem: in the case where k is the number of samples in the trace, then CPM will play back the trace exactly, which does not allow representative simulation.

Our CPM implementation uses a hashtable to store the CPM state space, where the key is a string concatenation of the noise values and the value is the PDF. We found that $k = 10$ provides a good tradeoff between being representative of the noise yet remaining non-deterministic, as determinism could lead to incorrect assumptions when testing protocols. We consider a more complete examination of k as an important area of future work.

3.4 Correlation Distortion Method

The main cause of interference we observed, 802.11, has a non-Gaussian property as a result of its discrete traffic patterns. The tradeoff k imposes in CPM raises a significant issue: much of the periodic noise spikes (e.g., 802.11 beacons) have very long periods. For CPM to be able to capture these beacons, for example, k should be larger than or equal to 100. This large k (100ms) makes the CPM state space very sparse. There is longer-term correlation in the noise trace, but CPM cannot effectively capture it. Our third approach addresses this limitation by using a non-Gaussian random process, which captures longer-term periodicities.

The core idea of the method is to transform non-Gaussian to Gaussian with the same auto-correlation or spectrum of target. Expressing the relationship in terms of Hermite polynomials allows us to generate Gaussian random process by using spectral representation method. In the end, with the generated Gaussian process, the original non-Gaussian process can be achieved by using a transformation equation (Eq. (8)).

Noise	Mean	Std	Skewness	Kurtosis
Real Noise	-97.1017	2.9702	3.8350	23.2346
Simul. Noise	-97.6699	2.0886	5.1972	49.3293

Table 2: Statistical characteristics of real noise in a light Meyer trace and noise correspondingly simulated using the correlation distortion method.

More formally, we apply the correlation distortion method [7, 8, 13] to generate a non-Gaussian random process with a prescribed auto-correlation function. We calculate the auto-correlation of the random process from a noise trace using mean-square (MS) ergodicity, assuming that the noise random process follows wide-sense stationarity. A non-Gaussian random process $x(t)$ has a nonlinear relationship with a Gaussian normal random process $u(t)$, i.e. $x(t) = g(u(t))$. In Eq. (1), the auto-correlation of non-Gaussian process in terms of that of Gaussian normal random process can be described as

$$R_{uu}(\tau) = \sum_{k=0}^{\infty} a_k^2 \rho_{xx}^k(\tau) \tag{1}$$

$$where\ a_k = \frac{1}{\sqrt{2\pi k!}} \int_{-\infty}^{\infty} g(\sigma u)\ exp(-\frac{u^2}{2}) H_k(u) du \tag{2}$$

$$H_k(u) = (-1)^k exp(\frac{u^2}{2}) \frac{d^k}{du^k} [exp(-\frac{u^2}{2})]. \tag{3}$$

In the above expressions, ρ_{xx} is the normalized auto-correlation of the non-Gaussian process $x(t)$ and $H_k(u)$ is the k^{th} Hermite polynomial. The Hermite polynomial is a classical orthogonal polynomial basis function. With these mathematical relations, the simulation procedure in correlation distortion method is described in Figure 4. By Eq. 4, the auto-correlation of non-Gaussian process can be transformed into that of a Gaussian process.

$$R_{xx}(\tau) = \alpha^2 [R_{uu}(\tau) + 2\hat{h_3}^2 R_{uu}^2(\tau) + 6\hat{h_4}^2 R_{uu}^3(\tau)] \tag{4}$$

$$\hat{h_3} = \frac{\gamma_3}{4 + 2\sqrt{1 + 1.5\gamma_4}},\ \hat{h_4} = \frac{\sqrt{1 + 1.5\gamma_4} - 1}{18}$$

$$\alpha = \frac{1}{\sqrt{1 + 2\hat{h_3}^2 + 6\hat{h_4}^2}} \tag{5}$$

where γ_3 is skewness(3^{rd} order moment) of the process and γ_4 is kurtosis(4^{th} order moment) of the process.

One limitation in the standard Hermite Model is that $\hat{h_3}$, $\hat{h_4}$, and α parameters have been calculated with the assumption of small deviations from Gaussian. Therefore, for non-Gaussians which deviate significantly, the method is not quite applicable. To reduce this problem, we applied modified Hermite models in Eq. (6) and (7), which was proposed by Tognarelli et al. [22], leading to improvement of performance in non-Gaussian simulation.

$$\gamma_3 = \alpha^3 (8\hat{h_3}^3 + 108\hat{h_3}\hat{h_4}^2 + 36\hat{h_3}\hat{h_4} + 6\hat{h_3}) \tag{6}$$

$$\gamma_4 + 3 = \alpha^4 (60\hat{h_3}^4 + 3348\hat{h_4}^4 + 2232\hat{h_3}^2\hat{h_4}^2 + 60\hat{h_3}^2 + \tag{7}$$

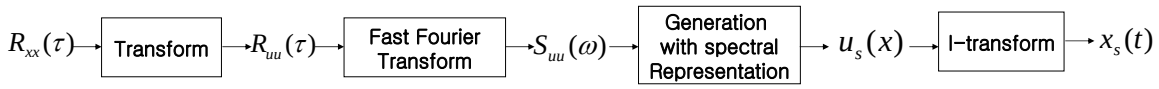

Figure 4: Correlation Distortion Method. By using the relationship between non-Gaussian and Gaussian random process, non-Gaussian random process can be generated via generation of Gaussian random process.

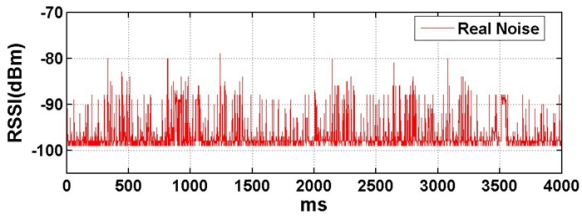

(a) Noise Traces of Real Noise for 802.11b low traffic

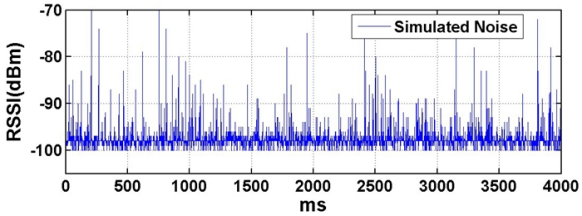

(b) Noise Traces of Simulated Noise by Correlation Distortion method for 802.11b low traffic

Figure 5: 4 second noise traces of real low traffic 802.11b noise and example simulated noise using the correlation distortion method. The simulated noise captures the periodic beacon signal and low traffic behavior.

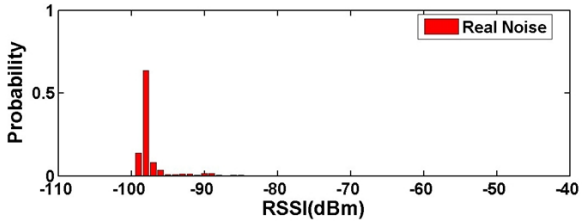

(a) First-order PMF for Real Noise for 802.11b low traffic

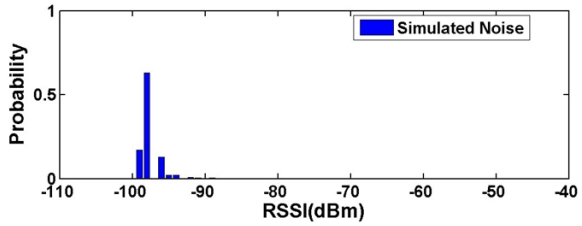

(b) First-order PMF for Simulated Noise by Correlation Distortion method for 802.11b low traffic

Figure 6: First-order PMF for real noise and simulated noise by correlation distortion method for low 802.11b traffic. They show the similar distribution of RSSI values.

$$252\hat{h_4}^2 + 1296\hat{h_4}^3 + 576\hat{h_3}^2\hat{h_4} + 24\hat{h_4} + 3)$$

$$x = \alpha[u + \hat{h_3}(u^2 - 1) + \hat{h_4}(u^3 - 3u)] \quad (8)$$

The correlation distortion method can generate noise data representative of a low-traffic 802.11b environment. Figure 5 shows simulated noise traces compared to real noise ones. This is because it can capture the long-term periodicities. We compared how well a simulated noise trace follows real noise behavior in terms of power spectral density corresponding to auto-correlation function, first-order PMF, mean (1^{st} moment), standard deviation(2^{nd} moment), skewness (3^{rd} moment), and kurtosis (4^{th} moment). The power spectral density of simulated noise matches that of real noise. This means that time-correlated noise information, which could be a critical factor for consecutive packet failures, is successfully exploited. For the first-order PMF, our simulated noise closely follows the RSSI distribution of real noise in Figure 6, but it is not exactly same as the real one. The Jensen-Shannon distance between PMFs of real noise and simulated noise is 0.089. While the naïve method in the above section can achieve the perfectly same first-order PMF, it fails to exploit time-correlated information. With a small difference of the first-order PMF, this approach achieves the sameness of auto-correlation between short-term noise data. Table 2 shows the mean, standard deviation, skewness, and kurtosis.

However, heavy-traffic 802.11b environments deviate significantly from Gaussian noise. The correlation distortion method is usually applicable to the environment of mediocre deviations from Gaussian. In Section 4, we compare the correlation distortion method to CPM and naïve sampling for low-traffic and heavy-traffic environments.

4. EXPERIMENTAL METHODOLOGY

We measure simulation accuracy by comparing conditional packet delivery functions (CPDFs). A conditional packet delivery function describes the probability that a packet will be received successfully given n previous failures or successes. For example, the CPDF of node A to node B c_{AB} of 5 ($c_{AB}(5)$) is the probability that B will receive a packet from A after 5 consecutive failures, while $c_{AB}(-5)$ is the probability that B will receive a packet after 5 consecutive successes. If packet losses are independent, then the CPDF is for the most part uniform; if packet losses are bursty, then the CPDF is non-uniform.

We compare CPDFs using a rigorous theoretical measure, the Kantorovich-Wasserstein distance. The Kantorovich-Wasserstein distance has been widely used in theoretical statistics and image signal processing applications to show the similarity of probability distributions. The Kantorovich-

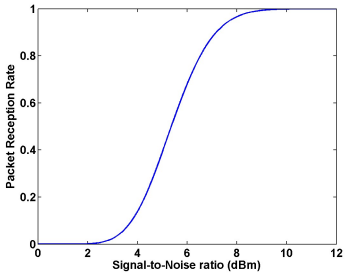

Figure 7: The CC2420 SNR/PRR curve.

Wasserstein metric is defined as

$$d_p^W(X^*, Y^*) = \inf_{\eta} \sqrt[p]{\frac{1}{N}\sum_{i=1}^{n}\sum_{i^*=1}^{n^*} d(x_i, y_{\eta 1(i,i*)})^p} \quad (9)$$

where $\eta : (i, i^*) \rightarrow (\eta_1(i, i^*), \eta_2(i, i^*))$.

To calculate the Kantorovich-Wasserstein distance as our evaluation metric, we used open-source codes for the Earth Movers Distance [18], which is equivalent to Kantorovich-Wasserstein distance. We use Kantorovich-Wasserstein rather the Chi-squared test because CPDF values are not independent, and rather than the Kolmogorov-Smirnov test because a CPDFs is a discrete rather than continuous function.

We use the Kantorovich-Wasserstein distance of CPDFs rather than measuring the noise itself because of the difficulty of comparing noise traces. Because our goal is to generate a representative and reusable model of an environment's noise, rather than simply replay it, simulated noise will inherently differ from the measured noise. We found that comparing mathematical properties of simulated and real noise gave some indications that they might lead to similar packet behavior, but for almost every similarity measure between noise traces it is simple to create a degenerate case that is mathematically similar but behaves completely differently. We therefore measure similarity in terms of the behavior we seek to recreate: packet delivery.

We use the real noise trace as a baseline for measuring the accuracy of different simulation methods. This allows us to control all other variables in an experiment. To generate the baseline CPDF, we use the real noise trace against an SNR curve derived from CC2420 experiments, using a fixed signal strength with a fixed inter-packet interval (15ms). While the signal strength is fixed for each simulation model, it is not fixed across the models, as models assume different sensitivity thresholds or SNR curves. Instead, for each model we choose the signal strength that creates a desired PRR. This way, we can evaluate how good, bad, and intermediate links manifest in each simulation model, given a particular noise environment. Evaluating them in this way asks the critical question "What do good, bad, and intermediate links look like to a simulated node?"

For example, the default radio model of TinyOS 2.x's TOSSIM (TOSSIM2) simulator samples noise values from the uniform distribution $[m - r, m + r)$. Given a trace, we compute the mean and variance of the noise values and use them as the mean and range of TOSSIM's RF model (this is not 100% accurate, but since noise does not follow a uniform distribution, we believe it to be a reasonable approximation). We then tune the signal strength until it has the desired PRR (e.g., 51% for an intermediate link, 90% for a good link). We do the same for the baseline: we tune the signal strength so that sampling from the PRR/SNR curve using the real noise trace has the same PRR. We measure PRR over a 195 second trace with an inter-packet interval of 15ms (135,000 packets).

Model	Naive Sampling	CPM	Corr.Dist.
Running Time	6 μs	14.2 μs	769 μs

Table 3: Mean execution time for each model to generate a noise sample.

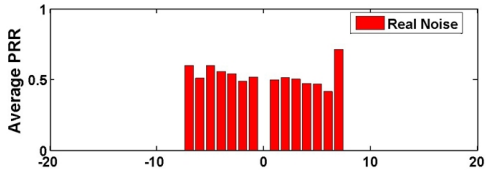

Figure 8: CPDF of an intermediate link from low-noise Meyer trace of real noise. The X-axis [-20,20] is consecutive packet delivery successes (negative) or failures (positive), and the Y-axis is the PRR. Packet losses are nearly independent.

We evaluate the noise models and four simulators: EmStar's shadowing model with uniformly random noise, TOSSIM's bit-error model [14], TOSSIM 2.x's gain model [4], and ns2's shadowing model with Gaussian random noise [1].

4.1 Noise Sampling

We used our noise sampling TinyOS application to gather data from a wide range of environments and 802.15.4 channels. Figure 1 showed three example traces. We also collected noise traces from the Grand Canyon in Arizona, Gates Hall at Stanford, and in the middle the Great Salt Desert. In the Grand Canyon and Great Salt Desert we observed no 2.4GHz noise besides AWGN; in Gates Hall we observed noise similar to Meyer Library.

4.2 Implementation

We incorporated our three noise models with combined path-loss and shadowing model into the TOSSIM simulator of TinyOS 2.0 [3]. Naive sampling keeps a probability distribution of a measured noise traces from a specific distance to 802.11b access point. CPM uses a hashtable to make an efficient query and derive a noise value by sampling from it. The correlation distortion method requires 1,024 data points in floating type, which include power spectral density information. After deriving an estimated noise value from three different methods with 1ms granularity, it is applied to combined path-loss and shadowing model. The packet delivery success or loss is determined by signal-to-noise by using signal-to-noise ratio curve in Figure 7. In order to separate out the effects noise have on packet delivery from the effects it has on media access, we disabled CSMA at the transmitter in all experiments (its noise is always below the clear channel threshold).

We measured the running time of each of our simulation models, shown in Table 3. We measured these values under Cygwin using `gettimeofday(2)` on a Fujitsu S6000 laptop with a 1.6GHz Pentium M processor. Both the naive sampling and CPM approaches are very fast; we do not expect them to be a significant bottleneck in packet-level simulation. The correlation distortion method, in contrast, intro-

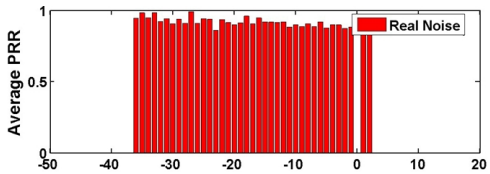

(a) Good Link (PRR = 90%)

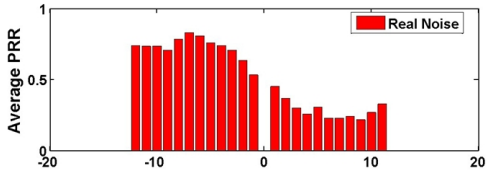

(b) Intermediate Link (PRR = 51%)

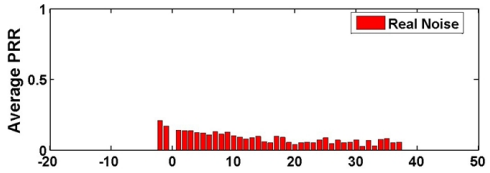

(c) Bad Link (PRR = 11%)

Figure 9: Conditional packet delivery functions for a good, intermediate, and poor link using the heavy use Meyer library trace. The X-axis is the consecutive packet delivery successes (negative) or failures (positive), and the Y-axis is the PRR. In a good link, losses are independent of prior behavior and in a poor link they are slightly correlated. In intermediate links they are highly correlated.

duces significant delays. Because our noise traces are 1kHz samples, we simulate noise at a 1kHz granularity. Currently we simulate noise as a continuous stream (take every sample). For large simulations with bursty traffic patterns this approach is inefficient, We are currently evaluating ways to avoid this cost (e.g., after $n \cdot k$ unsampled periods, revert to the mode distribution).

5. EVALUATION

We generated for many traces with a variety of signal strengths in order to measure packet delivery behavior for good, bad, and intermediate links. For the most part, low-rate traffic and quiet environments behave in a simple fashion: packet losses due to noise are independent. For example, packet losses from the Grand Canyon trace would be due to AWGN and the SNR curve, both of which cause independent losses rather temporally correlated bursts of loss. In low-rate conflicting traffic environments, clock skew as well as differing intervals between conflicting sources and sensor nodes make periodic losses possible but highly unlikely.

Figure 8 shows that for an intermediate link, packet losses are independent with respect to consecutive packet losses. This means that low 802.11b traffic does not lead to burst packet errors and the temporal effects can be negligible in low-traffic 802.11b environment. Therefore, other simulation methods cannot show the significant difference.

Traces taken in a busy 802.11 environment, however, behave differently. Figure 9 shows CPDFs for a good, intermediate, and bad link generated from the busy Meyer trace in

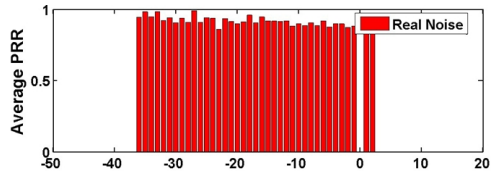

(a) Real Noise

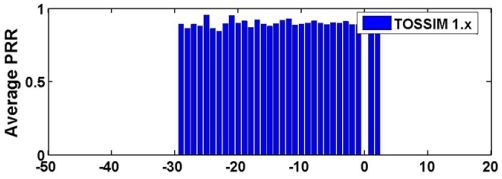

(b) TOSSIM 1.x

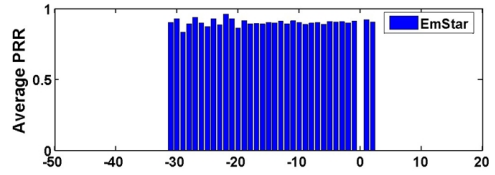

(c) EmStar

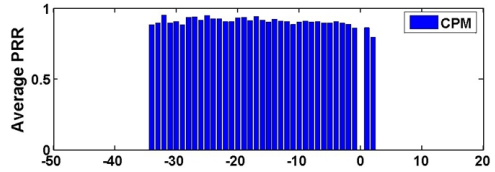

(d) CPM

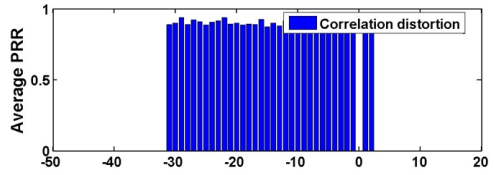

(e) Correlation Distortion

Figure 10: CPDFs of a good link from the busy Meyer trace of real noise, TOSSIM 1.x, EmStar, and Closest-fit Pattern Matching. The x-axis [-50,20] is consecutive packet delivery successes (negative) or failures (positive), and the Y-axis is the PRR.

Approach	KW
EmStar	0.1463
TOS 1.x	0.1902
TOS 2.x	0.2174
ns2	0.1935
Naive	0.1433
CPM	**0.0719**
Corr. Dist.	0.1440

(a) KW distances.

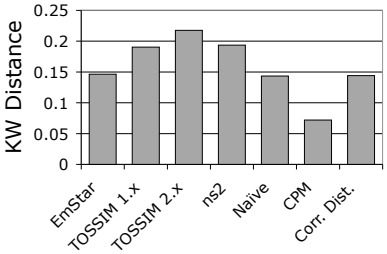

(b) KW distance plot.

Figure 11: Kantorovich-Wasserstein distance of simulation approaches from the real noise trace for a good link (PRR = 0.90).

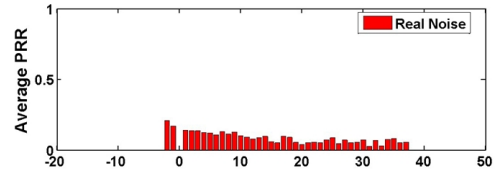

(a) Real Noise

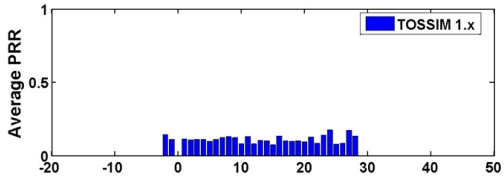

(b) TOSSIM 1.x

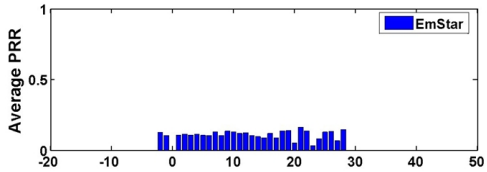

(c) EmStar

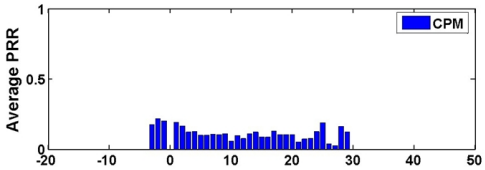

(d) CPM

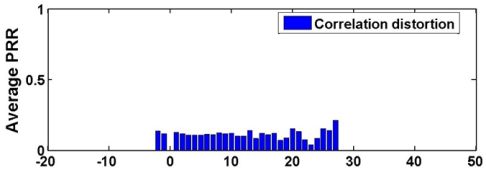

(e) Correlation Distortion

Figure 12: CPDFs of a bad link from the busy Meyer trace of real noise, TOSSIM 1.x, EmStar, and Closest-fit Pattern Matching. The x-axis [-20,50] is consecutive packet delivery successes (negative) or failtures (positive), and the Y-axis is the PRR.

Approach	KW
EmStar	0.0394
TOS 1.x	0.0394
TOS 2.x	0.0395
ns2	0.0352
Naive	**0.0322**
CPM	0.0394
Corr. Dist.	0.0412

(a) KW distances.

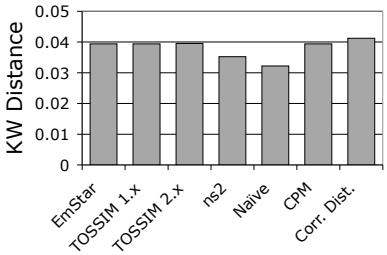

(b) KW distance plot.

Figure 13: Kantorovich-Wasserstein distance of simulation approaches from the real noise trace for a bad link (PRR = 0.11).

Figure 1. Despite the temporal correlation in noise, packet behavior in good and bad links is for the most part independent. In the case of a good link, this is due to the fact that the packet transmission interval (15ms) is not a factor of the large noise spikes, which are governed by TCP and HTTP timing. In the case of a bad link, there are many long bursts of loss caused by the web traffic, creating a long tail over which PRR degrades slightly. For an intermediate link, however, there is a pronounced correlation between prior and future losses: there is a 4-fold different in the loss rate after 6 delivery successes and 6 delivery failures.

Figure 10 shows how different simulation approaches capture the dynamics of a good link. Because losses are essentially independent, different simulation approaches all perform reasonably well. However, at high PRRs, slight variations can significantly change the CPDF. Note that the real noise trace has up to 36 consecutive packet delivery successes, while TOSSIM and EmStar only reach 29 and 32 respectively. In contrast, CPM reaches up to 35. Table 11 shows the Kantorovich-Wasserstein distance of the CPDFs of our three approaches as well as both versions of TOSSIM, ns2, and EmStar. CPM has the lowest KW distance (0.0719) by a factor of 2 (0.0719). Every approach had an identical PRR over the 130,000 packets of the 195s interval.

Figure 12 shows how different simulation approaches capture the dynamics of a poor link. Again, the different simulation approaches all perform reasonably well. However, CPM is able to short-term trends well enough to capture PRR degradation as losses increase. Table 13 shows the KW distance of the CPDFs of our three approaches and sensornet simulators. Naive sampling has a distance 10% lower than the next best approach, ns2. However, all approaches have KW distances within 0.009 of one another.

As Figure 9 shows, intermediate links are more complex than their good and bad counterparts. Unlike the comparatively flat CPDFs of good and bad links, an intermediate link can have a huge variation in PRR. This behavior supports the common observation that intermediate links are the difficult ones for networking algorithms such as link estimators. They are therefore the most interesting and important to simulate. Given the simplicity of other cases, we focus on intermediate links for the rest of the evaluation.

Figure 14 shows the CPDFs of an intermediate link based on real noise as well as using EmStar, TOSSIM 1.x, TOSSIM 2.x, ns2, naïve sampling, closest-fit pattern matching, and the correlation distortion method. For real noise in an intermediate link, the PRR decreases as the number consecutive packet losses increases. This represents the burstiness of the noise in this class of environment. One packet loss indicates that the node is likely encountering a packet burst, and therefore the PRR decreases for a reasonable period. The PRR values in response to packet successes indicate the probability of encountering a burst of loss. The PRR values given consecutive losses are non-zero because of 802.11b timing; it is possible to transmit 802.15.4 packets in between 802.11b/TCP timers.

All simulation models except CPM shows PRRs that are for the most part independent of consecutive packet delivery failures or successes: the CPDF converges to the average PRR value regardless of error bursts. CPM captures the short-term temporal effects, showing the same behavior as real noise. Table 15 shows the Kantorovich-Wasserstein distance of each CPDF with the real noise trace. CPM sig-

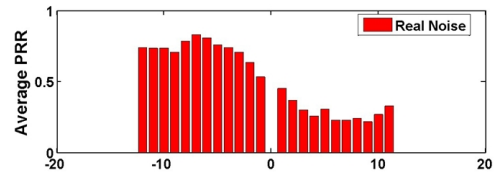

(a) Real Noise

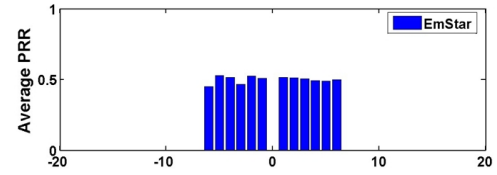

(b) EmStar

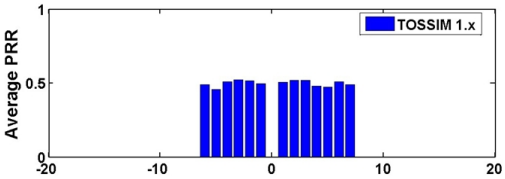

(c) TOSSIM 1.x

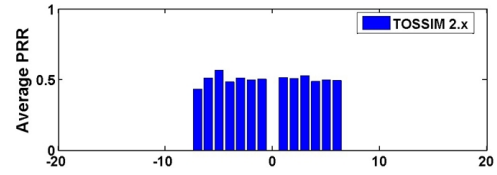

(d) TOSSIM 2.x

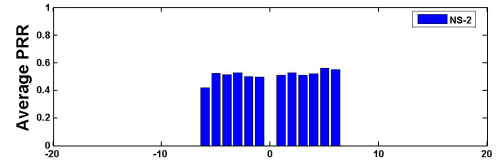

(e) ns2

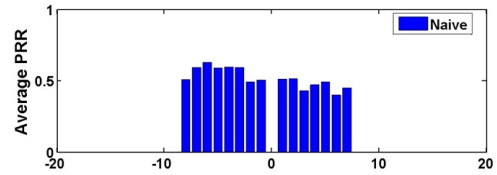

(f) Naive Sampling

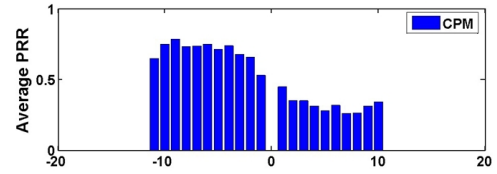

(g) CPM

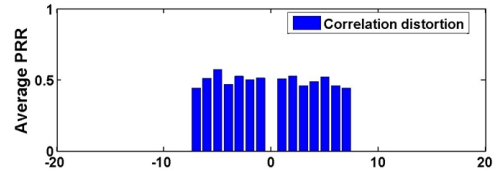

(h) Correlation Distortion

Figure 14: CPDFs of an intermediate link from the busy Meyer trace. The X-axis is consecutive packet delivery successes (negative) or failures (positive), and the Y-axis is the PRR.

Approach	KW
EmStar	0.3373
TOS 1.x	0.3384
TOS 2.x	0.3164
ns2	0.3446
Naive	0.2660
CPM	**0.0840**
Corr. Dist.	0.3120

(a) KW distances.

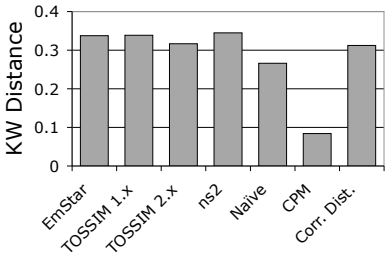

(b) KW distance.

Figure 15: Kantorovich-Wasserstein distance of simulation approaches from the real noise trace for an intermediate link (PRR = 0.51).

nificantly outperforms all other simulation methods.

Figure 8 shows that for an intermediate link, the CPDF does not show the same short-term effects under light 802.11b traffic as it does under heavy 802.11b traffic. The packet losses are independent with respect to the number of consecutive packet losses. This means that low 802.11b traffic does not lead bursts of packet errors: the temporal effects are negligible in low-traffic 802.11b environment.

The correlation distortion method's performance is markedly mediocre; it under performs naive sampling, and is very close to TOSSIM 2.x. Its strengths (and limitations) are in line with this observation; the advantage of the correlation distortion method is that it can accurately capture occasional spikes. Bursts of high noise, however, are too non-Gaussian for it to capture well. Unfortunately, occasional spikes generally appear as independent packet losses to to timing differences, and so the expressive power of this approach turns out to have very little benefit in practice.

Of the three techniques we proposed, CPM performs best. In our experiments, we set $k = 10$, packets are sent every 15ms and the noise sampling rate is 1kHz. This means that there will be ≈ 15 samples between two packet transmissions: the noise at one packet transmission is never in the historical window of the next transmission. CPM can capture bursts that span multiple inter-packet intervals, however, because the values it does consider are still dependent on those outside its window. Consider, for example, if CPM has a historical entry of this form:

$$PDF(8,8,8,8,8,8,8,8,8,8) = \{0.02 : 1, 0.98 : 8\}$$

That is, given 10 consecutive noise readings of 8, 2% of the time CMP will produce a noise value of 1 and 98% of the time a noise value of 98%. Once a run of 8s begins, the expectation is that it will last for 50ms (50 samples). In practice, CMP histories are much more complex, but the principle still holds.

6. DISCUSSION AND CONCLUSION

This paper takes a step forward in simulating packet delivery by modeling difficult noise signatures. However, modeling noise traces in this fashion makes three simplifying assumptions; relaxing each assumption is a complete research topic which we plan to explore.

First, by modeling each node's noise traces independently, these models ignore the fact that noise is spatially dependent. If node A hears a noise spike, nearby node B will hear it as well. In one formulation, this means that node A's noise

value not only depends on its prior noise values but also the noise values of its nearby neighbors. Capturing these dependencies requires information on where the noise sources are. Another formulation is to turn the problem around and simulate noise sources (rather than observed noise) and simply calculate the noise propagation in order to measure noise at each possible listener.

Second, while packet-based noise changes are abrupt and therefore contribute to short-term changes in SNR and correlated losses, there are also longer-term SNR changes due to gradual RSSI trends [16, 20]. Concurrently simulating both phenomena – brief noise spikes and long-term RSSI swings – would allow simulation to accurately capture both long-term and short-term dynamics. Furthermore, CPM only handles short-term noise bursts; characterizing longer-term noise trends (busy and quiet periods) would allow longer-running simulations that address another level of dynamism.

Finally, all of our results are based on a single (albeit dominant) low-power radio technology, and we have not observed all forms of 2.4GHz interference. Microwave ovens and analog 2.4GHz devices, for example, produce relatively long (seconds-minutes) periods of high interference, while Bluetooth's frequency hopping undoubtedly has complex and interesting dynamics. Evaluating our approaches in other ISM bands (e.g., the 433 and 915 MHz CC1000 radio on the mica2 platform) would better establish how general they are.

Our experimental results demonstrate that using an SNR curve with a closest-fit pattern matching noise model can significantly increase wireless packet delivery simulation accuracy. Furthermore, we can easily generate CPM models from real noise traces, allowing tools to effectively represent real-world environments in simulation. This approach shifts the focus from simulation algorithms to how well a simulation can capture real-world behavior based on real-world data, hopefully enabling researchers to evaluate and test protocols in a diverse set of representative environments.

Acknowledgements

This work was supported by generous gifts from the Intel Corporation and Docomo Capital, a fellowship from the Samsung Lee Kun Hee Scholarship Foundation, the National Science Foundation under grant #0615308 ("CSR-EHS"), and a Stanford Terman Fellowship.

7. REFERENCES

[1] The network simulator - ns-2. http://www.isi.edu/nsnam/ns.

[2] Sensor network emulator/simulator/debugger. http://www.cshcn.umd.edu/research/atemu/.

[3] Tinyos 2.0. http://www.tinyos.net/tinyos-2.x/.

[4] Tossim 2.x. http://www.tinyos.net/tinyos-2.x/.

[5] A. Cerpa, N. Busek, and D. Estrin. Scale: A tool for simple connectivity assessment in lossy environments. Technical Report 0021, Sept. 2003.

[6] A. Cerpa, J. L. Wong, M. Potkonjak, and D. Estrin. Temporal properties of low power wireless links: Modeling and implications on multi-hop routing. In *Proceedings of the Sixth ACM International Symposium on Mobile Ad Hoc Networking and Computing (MOBIHOC'05)*, 2005.

[7] D. Conner and J. Hammond. Modeling of stochastic system inputs having prescribed distribution and covariance functions. In *Applied Mathematical Modeling*, volume 3, 1979.

[8] R. Deutsch. *Nonlinear Transformations of Random Processes*. Prentice-Hall, 1962.

[9] D. Ganesan, B. Krishnamachari, A. Woo, D. Culler, D. Estrin, and S. Wicker. Complex behavior at scale: An experimental study of low-power wireless sensor networks. 2002.

[10] D. Ganesan, B. Krishnamachari, A. Woo, D. Culler, D. Estrin, and S. Wicker. An empirical study of epidemic algorithms in large scale multihop wireless networks. UCLA Computer Science Technical Report UCLA/CSD-TR 02-0013, 2002.

[11] L. Girod, T. Stathopoulos, N. Ramanathan, J. Elson, D. Estrin, E. Osterweil, and T. Schoellhammer. A system for simulation, emulation, and deployment of heterogeneous sensor networks. In *Proceedings of the 2nd international conference on Embedded networked sensor systems (SenSys)*, pages 201–213, New York, NY, USA, 2004. ACM Press.

[12] C. Givens and R. Shortt. A class of wasserstein metrics for probability distributions. volume 31, pages 231–240, 1884.

[13] G. Johnson. Constructions of particular random process. In *Proceedings of the IEEE*, volume 82, pages 270–285, 1994.

[14] P. Levis, N. Lee, M. Welsh, and D. Culler. TOSSIM: Simulating large wireless sensor networks of tinyos motes. In *Proceedings of the First ACM Conference on Embedded Networked Sensor Systems (SenSys)*, 2003.

[15] P. Levis, N. Patel, D. Culler, and S. Shenker. Trickle: A self-regulating algorithm for code maintenance and propagation in wireless sensor networks. In *First USENIX/ACM Symposium on Network Systems Design and Implementation (NSDI)*, 2004.

[16] S. Lin, T. He, J. Zhang, G. Zhou, L. Gu, and J. A. Stankovic. Atpc: Adaptive transmission power control for wireless sensor networks. 2006.

[17] S. Ratnasamy, B. Karp, L. Yin, F. Yu, D. Estrin, R. Govindan, and S. Shenker. Ght: a geographic hash table for data-centric storage. In *Proceedings of the first ACM international workshop on Wireless sensor networks and applications*, pages 78–87. ACM Press, 2002.

[18] Y. Rubner, C. Tomasi, and L. J. Guibas. A metric for distributions with applications to image databases. In *Proceedings of the 1998 IEEE International Conference on Computer Vision*, pages 59–66, 1998.

[19] D. Son, B. Krishnamachari, and J. Heidemann. Experimental study of concurrent transmission in wireless sensor networks. In *Proceedings of the Fourth ACM Conference on Embedded Networked Sensor Systems (SenSys)*, 2006.

[20] K. Srinivasan, P. Dutta, A. Tavakoli, and P. Levis. Understanding the causes of packet delivery success and failure in dense wireless sensor networks. In *Technical report SING-06-00*, Stanford, CA, 2006.

[21] B. L. Titzer, D. K. Lee, and J. Palsberg. Avrora: scalable sensor network simulation with precise timing. In *IPSN '05: Proceedings of the 4th international symposium on Information processing in sensor networks*, page 67, Piscataway, NJ, USA, 2005. IEEE Press.

[22] M. Tognarelli and A. Kareem. Equivalent statistical cubicization: A frequency domain approach for nonlinearities in both system and forcing function. In *Journal of Engineering Mechanics, ASCE*, volume 123, 1997.

[23] J. Zhao and R. Govindan. Understanding packet delivery performance in dense wireless sensor networks. In *Proceedings of the First International Conference on Embedded Network Sensor Systems*, 2003.

[24] M. Zuniga and B. Krishnamachari. Analyzing the transitional region in low power wireless links. In *First IEEE International Conference on Sensor and Ad hoc Communications and Networks (SECON)*, 2004.